Research Article

Esmaeel Zanganeh*, Mingzhao Song*, Adrià Canós Valero, Alexander S. Shalin, Elizaveta Nenasheva, Andrey Miroshnichenko*, Andrey Evlyukhin and Polina Kapitanova

Nonradiating sources for efficient wireless power transfer

Abstract: Nonradiating sources of energy realized under a wave scattering on high-index dielectric nanoparticles have attracted a lot of attention in nano-optics and nanophotonics. They do not emit energy to the far-field, but simultaneously provides strong near-field energy confinement. Near-field wireless power transfer technologies suffer from low efficiency and short operation distance. The key factor to improve efficiency is to reduce the radiation loss of the resonators included in the transmitter and receiver. In this paper, we develop a wireless power transfer system based on nonradiating sources implemented using colossal permittivity dielectric disk resonator and a subwavelength metal loop. We demonstrate that this nonradiating nature is due to the hybrid anapole state originated by destructive interference of the fields generated by multipole moments of different parts of the nonradiating source, without a contribution of toroidal moments. We experimentally investigate a wireless power transfer system prototype and demonstrate that higher efficiency can be achieved when operating on the nonradiating hybrid anapole state compared to the systems operating on magnetic dipole and magnetic quadrupole modes due to the radiation loss suppression.

1 Introduction

Rapid development of all-dielectric nanostructures has provided a new platform for nano-optics and photonics. The main mechanism to manipulate and control the light propagation at the nanoscale is based on the mode interference and electromagnetic field enhancement of optical resonators made of high-index dielectric materials. Different approaches to manipulate the light–matter interaction, such as engineering dielectric nanostructures with plasmonic materials [1], nanoparticle crystals [2], have been demonstrated so far [3, 4].

Recently, in electrodynamic problems much attention has been paid to the utilization of nonradiating (NR) electromagnetic sources, which have found a plethora of applications in photonics [5–12]. An NR source can be defined as a special kind of electromagnetic state that does not emit energy to the far-field region, but simultaneously provides strong near-field energy confinement [5]. Currently, two kinds of NR sources are at the center of intense theoretical and experimental investigations in photonics, the so-called anapole states, as well as Bound States in the Continuum (BICs). Owing to the nonexistence theorem [13], perfect BICs cannot occur in isolated photonic structures, where only the former (anapole states) can lead to far field suppression. Therefore, in the rest of this

*Corresponding authors: Esmaeel Zanganeh, School of Physics and Engineering, ITMO University, Saint Petersburg, 197101, Russia,
E-mail: esmaeelzanganeh@gmail.com. https://orcid.org/0000-0003-2580-4753; **Mingzhao Song**, School of Physics and Engineering, ITMO University, Saint Petersburg, 197101, Russia; and College of Information and Communication Engineering, Harbin Engineering University, Harbin, 150001, China,
E-mail: kevinsmz@foxmail.com. https://orcid.org/0000-0002-1264-4335; and **Andrey Miroshnichenko**, School of Engineering and Information Technology, University of New South Wales, Canberra, ACT, 2600, Australia, E-mail: andrey.miroshnichenko@unsw.edu.au. https://orcid.org/0000-0001-9607-6621
Adrià Canós Valero and Polina Kapitanova, School of Physics and Engineering, ITMO University, Saint Petersburg, 197101, Russia. https://orcid.org/0000-0003-3870-6351 (A.C. Valero). https://orcid.org/0000-0001-7315-4316 (P. Kapitanova)
Alexander S. Shalin, School of Physics and Engineering, ITMO University, Saint Petersburg, 197101, Russia; Riga Technical University, Institute of Telecommunications, Riga, 1048, Latvia; and Kotel'nikov Institute of Radio Engineering and Electronics of Russian Academy of Sciences (Ulyanovsk Branch), Ulyanovsk, 432000, Russia
Elizaveta Nenasheva, Ceramics Co. Ltd, 10, Kurchatova St., Saint Petersburg, 194223, Russia
Andrey Evlyukhin, Institute of Quantum Optics, Leibniz University Hannover, Welfengarten 1, 30167, Hannover, Germany; and Moscow Institute of Physics and Technology, Dolgoprudny, 141700, Russia. https://orcid.org/0000-0002-1801-6778

work, we refer to NR sources indistinctly as anapole states. Ordinary anapole states arise due to the destructive interference between the fields generated by the electric and toroidal dipole moments sharing the same far field characteristics [10, 14, 15]. In the last years, the latter have been found to take place in the scattering response of dielectric nanoparticles illuminated by an incident wave, rendering them invisible in the far-field region [10]. The concept has been generalized to the interference between the fields generated by other types of current distributions, such as the magnetic dipole with its toroidal counterpart [16], also higher order anapole states [17] and hybrid anapole states of mixed electric and magnetic character [18] were reported. Interestingly, it has been shown that the anapoles and hybrid anapoles can be constructed with ordinary multipoles, in the absence of toroidal contributions [19].

In the radiation/emission problem, ordinary anapole states were also studied in a structure comprised of four high refractive index dielectric cylinders excited by an electric dipole antenna [20] or a subwavelength dielectric sphere excited by a point-like antenna [21]. Other approach to realize an anapole state has been recently proposed in [22], where the nonradiating sources composed of a single ultrahigh permittivity dielectric hollow disk excited by electric or magnetic point-like dipole antennas, placed inside the inner hole were studied. It was experimentally demonstrated that the anapole effect can be used to significantly suppress the radiation losses with saving the energy in the near-field region. It is associated with the nonlocal near field distribution including longitudinal "attached" components of electromagnetic fields [23].

Evidently, the main advantage of NR sources is the far-field radiation suppression. The main question is what is it good for and what kind of applications can benefit from it? Recently, wireless power transfer (WPT) has become a key technology that needs to be developed urgently today [24, 25]. Near-field WPT method based on resonant magnetic coupling of the same resonance coils [26] aims to enlarge transfer distance and increase power transfer efficiency (PTE). However, such type of WPT systems suffers from high ohmic and radiative losses [27]. To solve the problem of reduced PTE caused by the ohmic loss in the metal coils, the Q-factor should be increased. For that purpose, high-permittivity low-loss dielectric resonators possessing magnetic Mie type resonances were proposed, and the WPT systems based on them were experimentally studied [28, 29]. However, the Q-factors of the low-order magnetic Mie resonances are still limited due to the efficient coupling with the radiative continuum. Thus, the high-Q quasi magnetic BIC supported by a dielectric metasurface was developed for the WPT application [30]. To date, however, the full potential of applying NR sources based on anapole state supported by a single dielectric resonator for the WPT application is still an open question not addressed yet.

The goal of this study is to develop a novel approach for highly-efficient near-field WPT via utilization of an NR source based on hybrid anapole state with strongly suppressed far-field radiation. The NR source is composed of a single colossal permittivity dielectric resonator excited by a small metallic loop situated in the near proximity as shown in Figure 1a. We demonstrate that the hybrid anapole state originates by destructive interference of the fields generated by multipole moments of different parts of the NR source, without a contribution of toroidal moments. For that we apply the secondary multipole analysis [31]. We also perform numerical simulation and experimentally demonstrate the NR source in the MHz frequency range. As a result, we design and experimentally verify a new WPT system possessing a high PTE, with virtually negligible radiative losses in comparison with other more conventional schemes.

2 Nonradiating source based on hybrid anapole state

Here, we study the NR source composed of a colossal permittivity dielectric disk and a metallic loop as shown in Figure 1a. We consider the colossal permittivity $\epsilon = 1000$ and low loss factor $\tan \delta = 2.5 \times 10^{-4}$ of the dielectric disk [32, 33]. The dielectric disk radius and height are $R = 42 \pm 0.05$ mm and $h = 4.2 \pm 0.05$ mm, respectively. A copper loop with the radius of $R_0 = 36$ mm and wire radius of 2 mm were used as a point-like antenna to excite the dielectric disk resonator.

Initially, we numerically studied the reflection coefficient, radiated power, stored electric and magnetic energies inside the dielectric disk, and losses of the NR source in CST Microwave studio as described in Section 5. At the frequencies 278 and 408.6 MHz we revealed the minima of the reflection coefficients which mean that all the input power couples to the dielectric resonator. There exist only three mechanisms of dissipation; namely, loss in dielectrics, loss in metals and loss in radiation (radiated power). At the frequency 278 MHz the simulated reflection coefficient becomes almost zero. The dielectric, metal losses and radiated power at this frequency are listed in Table 1 in Section 5. One can see that the structure radiates 0.42 W of power, while the rest is lost in dielectric and metal. The electric
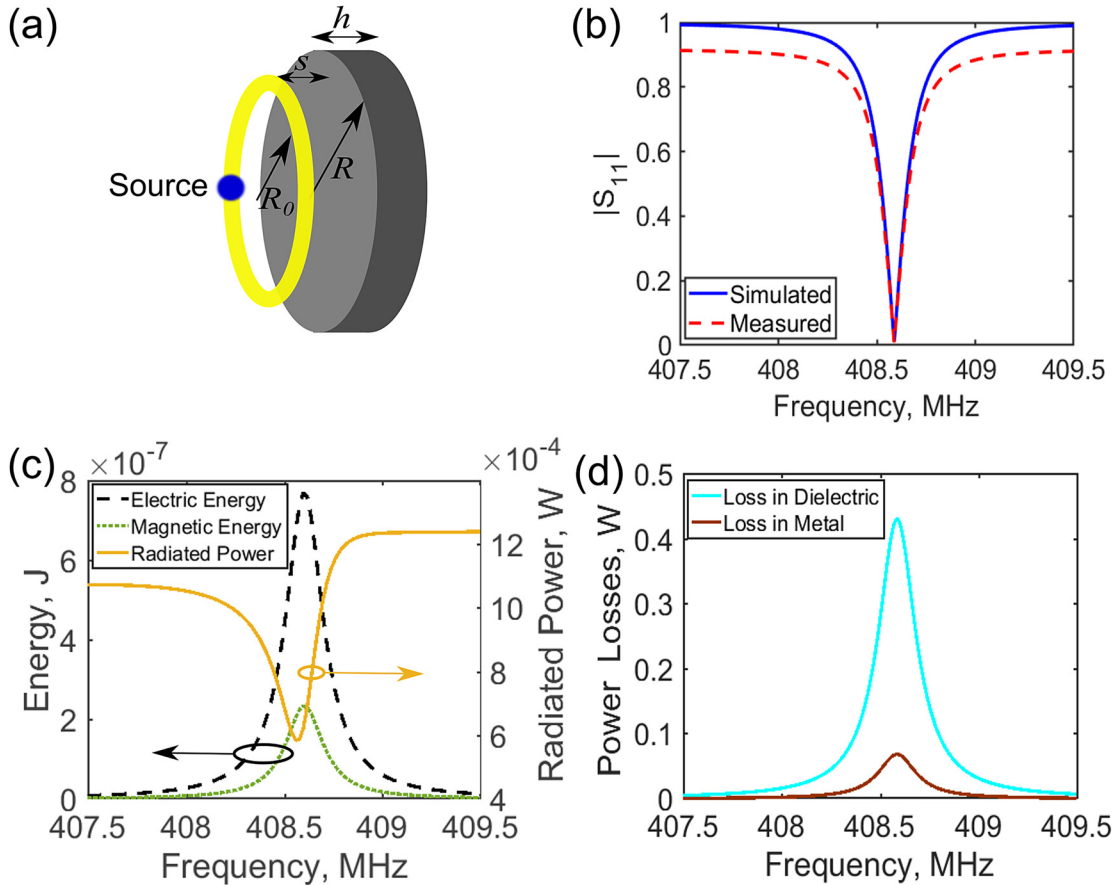
Figure 1: NR source design.
(a) Schematic view of the NR source. (b) Simulated and measured reflection coefficients. (c) Calculated electric and magnetic energies inside the dielectric disk and radiated power of the NR source. (d) Simulated power losses in dielectric and metal of the NR source.

Table 1: Geometrical parameters, resonant frequencies, losses and radiated power of the dielectric disk resonator excited with metal loop operating on MD, MQ and NR modes.

Mode	h (mm)	s (mm)	f (MHz)	Dielectric loss (W)	Metal loss (W)	Radiated power (W)
MD	4.2	42	278	0.078	0.002	0.42
MQ	10	2	508	0.45	0.0035	0.0465
NR	4.2	0.3	408.6	0.4305	0.069	0.0005

field is confined and swirling inside the resonator. The magnetic field is perpendicularly penetrating inside and out of the resonator indicating that the magnetic dipole (MD) moment (mode) is excited at this frequency [29]. At the frequency 408.6 MHz the simulated reflection coefficient is also near zero (see Figure 1b). The simulated values of radiated power and dielectric and metal losses are shown in Figure 1c and d, and listed in Table 1 in Section 5. Important to mention that almost zero Watt of the input power is lost as radiation. It means that the structure at this frequency became nonradiating and the stimulated

power is kept in the near-field. Around 90% of the input power is lost in dielectric and 10% in metal. The calculated electric and magnetic energies inside the dielectric disk are shown in Figure 1c (see Section 5) indicating the energy concentration inside the disk at the frequency of 408.6 MHz. The simulated near field distribution at the frequency 408.6 MHz demonstrates four closed loops of the electric field oscillating in the plane of the resonator (Figure 2a) with four maximums of magnetic field perpendicularly penetrating inside and out of the resonator (Figure 2b). Analyzing the obtained field distribution one
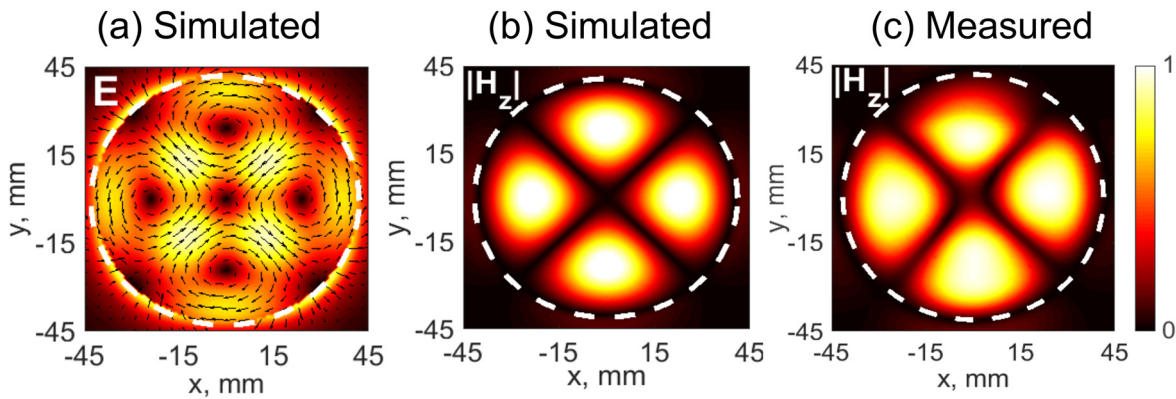
Figure 2: Near-field distributions of NR source at the frequency of 408.6 MHz.
(a) Simulated electric field, (b) simulated and (c) measured normal component of the magnetic field distribution of the NR source. The fields are shown 2 mm above the dielectric disk surface. The filed magnitudes are normalized to the maximum field intensity value (Maximum of the simulated electric field is 4628 V/m and maximum of the Z component of the simulated magnetic field is 152 A/m.). The white dashed lines represent the dielectric disk radius.

could say that at the frequency 408.6 MHz we observe the electric quadruple (EQ) moment (mode) excitation. However, the zero radiated power is not associated with this EQ mode. Together with the fact of energy accumulation inside the dielectric disk, we assume the the anapole state is formed at this frequency.

To gain a deeper understanding, we performed the Cartesian multipole expansion of the EM fields generated by the NR source with respect to the disk center (see Section 5 for details). Its (disk + Loop) total radiated power obtained in CST Microwave Studio and the corresponding contributions of electric dipole (ED), MD, EQ, magnetic quadrupole (MQ), and sum of the multipoles radiation are shown in Figure 3a. The sum of the multipoles radiation agrees well with radiated power obtained by CST Microwave studio simulation. At the frequency 408.6 MHz the dominant radiating moment is MD which also has a

strong dip at this frequency. The EQ and MQ have local small resonant contributions at this frequency.

To achieve more information, the radiation from the different parts of NR source, namely dielectric disk and the loop were separately decomposed to multipoles, also calculated with respect to the disk center, and the result is depicted in Figure 3b. The separate radiation contributions of ED moments of the disk and loop have more or less equal magnitude at the frequency of 408.6 MHz. At the same time, their radiated power is about 70 times larger than the radiated power from ED of the whole NR source indicated as ED in Figure 3a. Moreover, the phase difference between ED radiation from the loop and ED radiation from the disk resonator is π all over the frequency range (see Figure 3c). It means that the ED radiations from the loop and disk destructively interfere with each other in the far-field, suppress the radiation of the ED channel and
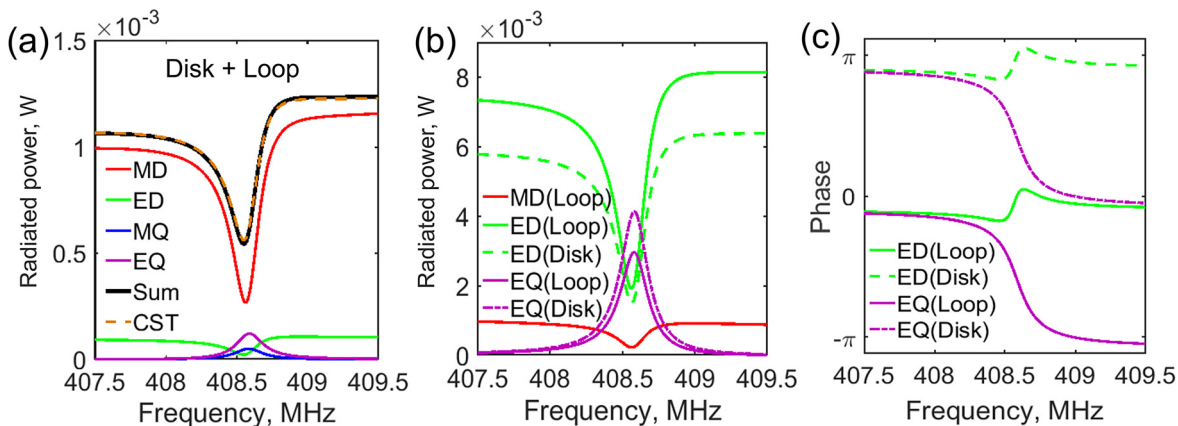
Figure 3: Cartesian multipole decomposition of radiated power of (a) the NR source (disk + loop); (b) the single dielectric disk and loop of the NR source; (c) phase of the ED and EQ radiations from the loop and disk.

form an *electric dipole* anapole state at this frequency. Similar radiation suppression of the EQ channel is observed as well; radiation of EQ (loop) and EQ (disk) are almost equal (Figure 3b) and out of phase (Figure 3c). The radiated power obtained for the dielectric disk and loop separately is about 40 times larger than the EQ radiation of the NR source indicated as EQ in Figure 3a. Therefore, the *electric quadrupole* anapole state also exists at the frequency 408.6 MHz. It is worth noting that the weak MD radiated from the NR source is exactly the same as the MD radiation of the loop. That means the MD radiation totally comes from the radiation of the loop and this moment is not excited in the disk resonator at all. Also, the MD is the dominant radiation channel of the NR source at the frequency of 408.6 MHz and its amount is 2.6×10^{-4} W. Note, that the dominant MD radiation and total radiation shown in Figure 3a are much smaller than the powers of the radiations which would be generated by ED and EQ moments of the disk and loop separately, see Figure 3b. Based on the results on numerical simulation and multipole decomposition, one can say that at the frequency of 408.6 MHz the NR source provides the nonradiating behavior associated with the hybrid anapole state formation resulted by the ED and EQ anapole states spectral overlap. For simplicity, later in the paper we will call the frequency of the hybrid anapole state (408.6 MHz) as the NR mode.

To prove our numerical prediction, the NR source has been fabricated and its EM characteristics have been measured (see Section 5). The measured reflection coefficient agrees well to the simulated one as shown in Figure 1b. The magnetic field distribution above the NR source has been also detected (see Figure 2c). As was predicted in Figure 2b by numerical simulations four maximum of the magnetic field are experimentally observed at the frequency of the NR mode. We also measured the magnetic field distribution of the NR source in the near-field region. The

50×50 cm^2 plane perpendicular to the NR source surface was investigated and the results were compared to the simulated magnetic field distributions including other resonant frequencies. At the MD mode the magnetic field of the structure has one maximum in the dielectric disk center as shown in Figure 4a. The intensity of the magnetic field is quite high and smoothly decays with the distance above the structure. It means that the power is leaking to the far-field. At the MQ mode the magnetic field has two maximums in the dielectric disk center (see Figure 4b). The field intensity is smaller than at the MD case and decays faster with the distance along z direction. At the NR mode we also observe two magnetic field maximums in the dielectric disk center (Figure 4c and d). However, in comparison to the previous two cases the magnetic field is strongly confined in the close proximity of the NR source. It means that almost no power is radiated to the far-field in contrast to the single MD and MQ modes.

3 Nonradiating WPT system

The proposed NR source was applied as the transmitter and receiver of a WPT system. We assume that the nonradiating behavior of the transmitter and receiver will cancel the far-field radiation and, as a result, enhance the PTE. It should be noticed that the efficiency enhancement will happen only at some certain separation between the transmitter and receiver while the optimal coupling is reached. Thus, we numerically and experimentally studied the NR WPT system based on two identical NR sources separated by distance d as shown in Figure 5. During the investigations, we numerically simulated and experimentally measured the S-parameters of the system and calculated the PTE as a function of the separation distance d (see Figure 6 and Section 5). In case of lossless metals and dielectric materials the PTE of the system operating at NR mode is 100%.
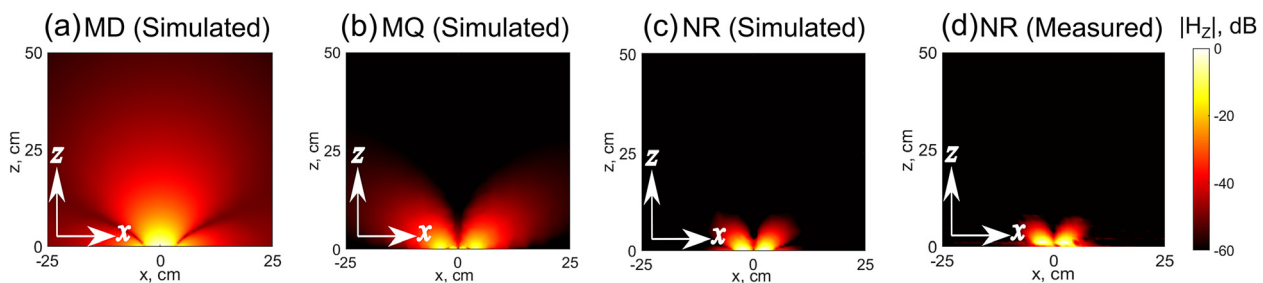

Figure 4: Simulated normal component of the magnetic field distribution at $x-z$ plane perpendicular to the dielectric disk surface on (a) MD, (b) MQ, and (c) NR modes. (d) Measured normal component of the magnetic field distribution corresponding to NR resonance at the frequency 408.6 MHz. The simulated fields magnitudes are normalized to MD maximum on the panel (a) and the measured field values on NR resonance is normalized to itself maximum value.

(a)

(b)
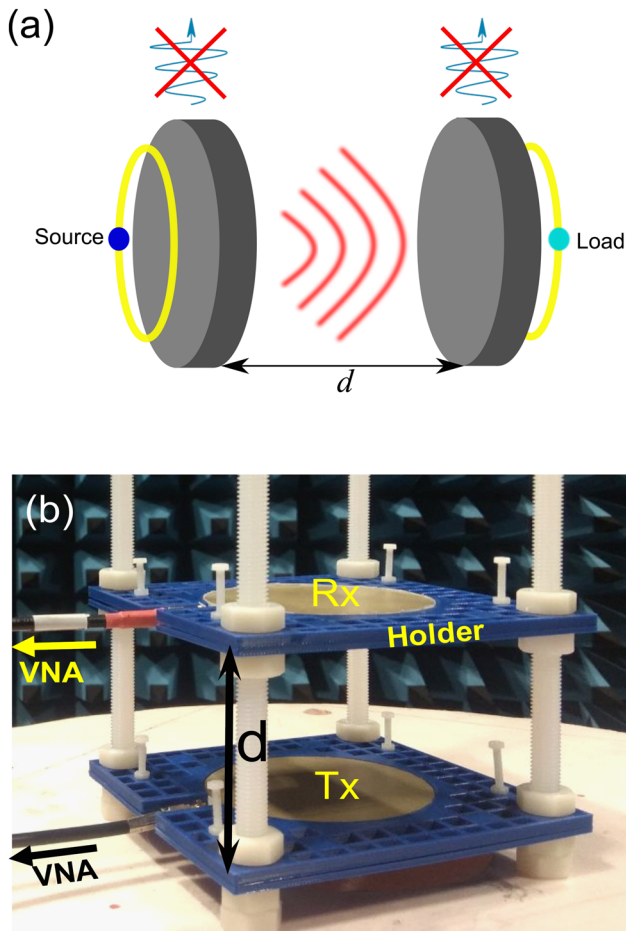
Figure 5: NR WPT system design.
Schematic view (a) and experimental setup (b) of the NR WPT system.

It decays when normalized distance reaches 13. It can be associated with the loosely coupling between the transmitter and receiver. However, the efficiency of the lossless WPT system operating on MD mode decreases faster as the operation distance increases due to the presence of the radiation losses. The introduction of the losses in metal and dielectric parts results in the decreasing of the maximal PTE values. Thus, the maximum PTE of the system on the NR mode reaches 95% while on the MD mode the PTE is 94%. However, the general trend of the curves persists with increasing of the normalized distance. The PTE on the MD mode decays faster which can be explained by higher radiation loss. The PTE of the system operating on the MQ mode is also plotted for comparison. The maximum PTE on the MQ mode is 82% which is lower than the maximal PTE on the NR and MD modes. It is due to the lower coupling coefficient and higher loss in dielectric parts and radiation.

To verify the simulated results we experimentally studied the WPT system characteristics (see Section 5 for details). Figure 7a and b show the simulated and measured
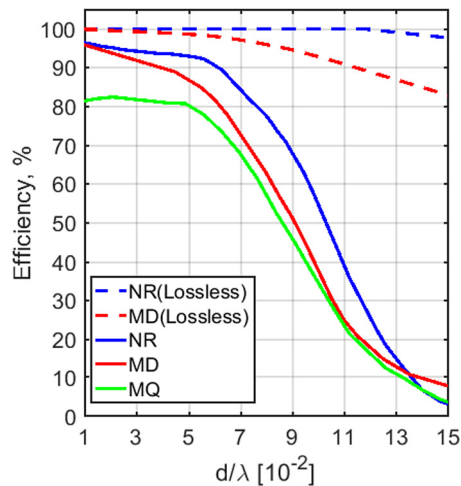
Figure 6: Results of numerical simulations of the WPT system: comparison of WPT efficiencies (calculated by Eq. (1)) of proposed system operating at NR, MD, and MQ modes as functions of the power transfer distance, which is normalized separately by their operational wavelengths λ.

S-parameters of the WPT system for two specific separation distances d. For $d = 6$ cm, the optimal coupling conditions are satisfied and we observe a single maximum of the transmission coefficient. For separation $d = 3$ cm, we observe the frequency splitting phenomena when the transmission coefficient has two maxima. It can be explained by the strong coupling between the transmitter and receiver. This phenomenon has also been observed earlier for WPT systems operating on the MD and MQ modes [28, 29]. The measured PTE as a function of the separation d is presented in Figure 7c in comparison to the results obtained by numerical simulations of the lossy WPT system operating on the NR mode. A good agreement is observed. A slight difference is resulted from the influence of rather massive plastic holder, which was not been taken into account during the numerical simulations. The measured efficiency of 92% is reached when the separation d is up to 4 cm (0.95 radii of the NR source). For comparison, the PTE of the WPT systems reported in [29] and [28] at the distance of 0.95 radii of the resonator are 90 and 80%, respectively. The PTE decays with the increase of the separation d which can be explained by the decrease of the coupling coefficient between the transmitter and receiver. However, PTE of 50% is observed at 7 cm separation distance.

A straightforward way to reveal power transfer from the transmitter to receiver and radiation loss in a WPT system is to analyze the Poynting vector streamlines. Poynting vectors for the WPT systems operating on the NR and MD modes for operation distances of $d/\lambda = 0.08$ were calculated using CST Microwave Studio post-processing tool and
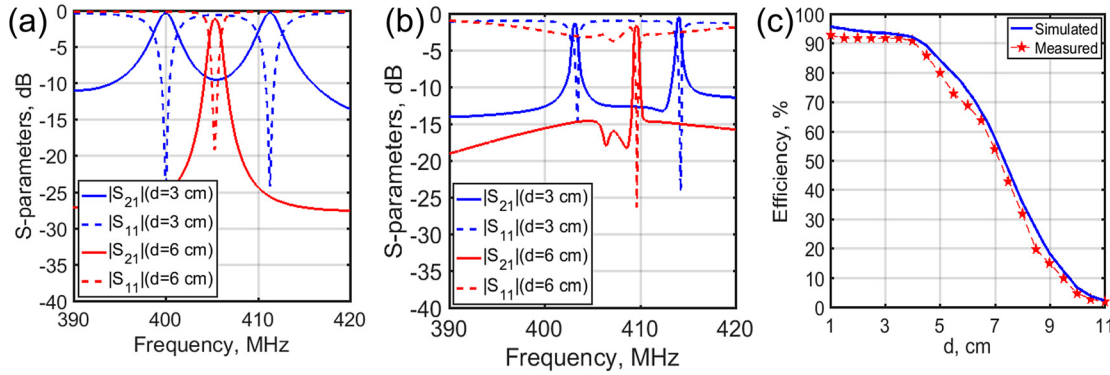
Figure 7: Measured and simulated characteristics of the NR WPT system as a function of separation *d*.
(a) Simulated and (b) measured S-parameters of the WPT system operating at the NR mode. (c) The measured and simulated power transfer efficiency.

are compared in Figure 8. In the NR WPT system, all the streamlines originate on the transmitter, and most of them terminate on the receiver (Figure 8a). It means that almost all the power flow that leaves the transmitter reaches the receiver and the radiation loss is barely visible, as almost no Poynting vector streamline goes to infinity. For the MD-WPT system, all the streamlines originate on transmitter,

but significant portion of them go to infinity (Figure 8b). Thus, this part of the power dissipates as the radiation and never reaches the receiver.

4 Conclusions

We have proposed and studied an NR source based on a colossal permittivity dielectric disk resonator excited by a subwavelength metal loop antenna. The nonradiating feature has been achieved by the formation of the hybrid anapole state due to the radiation cancellation between ED and EQ channels. We have fabricated the NR source prototype and experimentally confirmed the NR features predicted analytically and numerically. The WPT system composed of two NR sources acting as a transmitter and a receiver has been numerically and experimentally studied. We have demonstrated that the maximum PTE of 92% has to be obtained by getting rid of the radiation loss in the transmitter and receiver. This value is higher than the maximum PTE of WPT systems operating on the MD and MQ modes (resonances).

5 Materials and methods

5.1 Theoretical study

The numerical simulation and optimization of the NR source EM characteristics have been performed in CST Microwave Studio 2020. The frequency domain solver was used to simulate reflection coefficient, near-field distribution, dielectric and metal losses and radiated power. The system under study was based on a colossal permittivity dielectric disk resonator excited by a subwavelength metal loop antenna. We consider the colossal permittivity $\varepsilon = 1000$ and low loss factor $\tan \delta = 2.5 \times 10^{-4}$ of the dielectric disk. The radius of the disk was set as
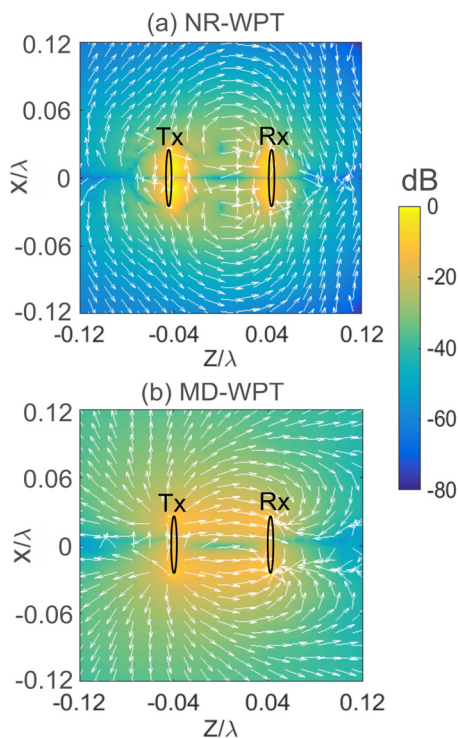
Figure 8: Poynting vector S streamlines and magnitude for (a) NR-WPT system at the frequency of 408.6 MHz and (b) MD-WPT system at the frequency of 278 MHz. Poynting vector magnitudes are normalized to their maximum values and shown in log scale. λ is the operation wavelength.

$R = 42$ mm. A copper loop with the radius of $R_0 = 36$ mm and wire radius of 2 mm have been used during the numerical simulations. It was placed at the distance s coaxially beside the disk. The 1 mm slit in the loop was created to insert a 50 Ω port in CST Microwave Studio. We have demonstrated numerically that optimization of the disk height and distance between the loop and the disk leads to excitation of different modes of the system. With respect to the results of numerical simulations one can find MD, MQ and NR modes at which we will get the minimum of the reflection coefficient. The geometrical parameters together with the resonant frequencies of the modes, level of losses and radiated power are listed in Table 1. We found that for disk height of 4.2 mm and distance between the disk and loop of 0.3 mm one can find a mode with almost zero radiation of power to the far-field zone.

The electric and magnetic energies demonstrated in Figure 1c were obtained from the simulated in CST Microwave Studio electric (E) and magnetic (H) field intensities by integrating them over the disk volume as follows: $W_E = \frac{\epsilon}{2} \int_V |E|^2 \, dv$ and $W_M = \frac{\mu}{2} \int_V |H|^2 \, dv$.

The Cartesian multipole expansion analysis in the long-wavelength approximation [34–36] is performed to show the origin of the NR source explicitly. The expressions used for radiated power in the multipole representation are presented in [35]. This approach is applied because the size of the system under study is much smaller than the wavelength of radiation. Here, we also use a secondary multipole analysis of full radiation [31] taking explicitly into account the separate contributions of the multipole moments of various parts of the NR source, namely the dielectric disk and the loop. All multipoles are calculated with respect to the disk center of mass. By integrating the current density within the dielectric volume and on the loop surface, the involved Cartesian multipoles are defined as [34, 35]:

$$P_\alpha^V = \frac{1}{i\omega} \int_V J_\alpha \, dv \tag{1}$$

$$P_\alpha^S = \frac{1}{i\omega} \int_S J_\alpha^S \, ds \tag{2}$$

$$P_\alpha = P_\alpha^V + P_\alpha^S \tag{3}$$

$$m_\alpha^V = \frac{1}{2} \int_V (r \times J)_\alpha \, dv \tag{4}$$

$$m_\alpha^S = \frac{1}{2} \int_V (r \times J^S)_\alpha \, ds \tag{5}$$

$$m_\alpha = m_\alpha^V + m_\alpha^S \tag{6}$$

$$Q_{\alpha\beta}^{(e)V} = \frac{1}{i\omega} \int_V \left(r_\alpha J_\beta + r_\beta J_\alpha - \frac{2}{3} \delta_{\alpha\beta}(r.J) \right) dv \tag{7}$$

$$Q_{\alpha\beta}^{(e)S} = \frac{1}{i\omega} \int_S \left(r_\alpha J_\beta^S + r_\beta J_\alpha^S - \frac{2}{3} \delta_{\alpha\beta}(r.J^S) \right) ds \tag{8}$$

$$Q_{\alpha\beta}^{(e)} = Q_{\alpha\beta}^{(e)V} + Q_{\alpha\beta}^{(e)S} \tag{9}$$

$$Q_{\alpha\beta}^{(m)V} = \frac{1}{3} \int_V [(r \times J)_\alpha r_\beta + (r \times J)_\beta r_\alpha] \, dv \tag{10}$$

$$Q_{\alpha\beta}^{(m)S} = \frac{1}{3} \int_V [(r \times J^S)_\alpha r_\beta + (r \times J^S)_\beta r_\alpha] \, ds \tag{11}$$

$$Q_{\alpha\beta}^{(m)} = Q_{\alpha\beta}^{(m)V} + Q_{\alpha\beta}^{(m)S} \tag{12}$$

where $\alpha, \beta = x, y, z$. The symbol P, m, $Q^{(e)}$, $Q^{(m)}$ represent electric dipole, magnetic dipole, electric quadrupole and magnetic quadrupole, respectively. δ is a delta Kronecker symbol. J^S is the surface current of the metallic loop, and J is the induced current density, which is defined inside the dielectric as follows:

$$J = i\omega\epsilon_0(\epsilon_r - 1)E \tag{13}$$

where ω is the angular frequency, ϵ_0 is the vacuum permittivity, ϵ_r is the complex relative permittivity of dielectric, and E is the electric field. Here, the time dependence is defined by exp ($i\omega t$). The total radiated power of these multipoles can then be calculated using:

$$P_{\text{rad}} = \frac{k^4}{12\pi\epsilon_0^2 c \mu_0} |P_\alpha|^2 + \frac{k^4}{12\pi\epsilon_0 c} |m_\alpha|^2$$
$$+ \frac{k^6}{160\pi\epsilon_0^2 c \mu_0} |Q_{\alpha\beta}^{(e)}|^2 + \frac{k^6}{160\pi\epsilon_0 c} |Q_{\alpha\beta}^{(m)}|^2 \tag{14}$$

μ_0 is the vacuum magnetic permeability. The multipole contributions to the radiated power appear below:

$$\text{Electric dipole (ED): } \frac{k^4}{12\pi\epsilon_0^2 c \mu_0} |P_\alpha|^2 \tag{15}$$

$$\text{Magnetic dipole (MD): } \frac{k^4}{12\pi\epsilon_0 c} |m_\alpha|^2 \tag{16}$$

$$\text{Electric quadrupole (EQ): } \frac{k^6}{160\pi\epsilon_0^2 c \mu_0} |Q_{\alpha\beta}^{(e)}|^2 \tag{17}$$

$$\text{Magnetic quadrupole (MQ): } \frac{k^6}{160\pi\epsilon_0 c} |Q_{\alpha\beta}^{(m)}|^2 \tag{18}$$

The numerical model of the WPT system based on two identical NR sources was created in CST Microwave Studio and studied numerically with the help of frequency domain solver. The reflection ($|S_{11}|$) and transmission ($|S_{21}|$) coefficients were numerically simulated and used to calculate the PTE as follows:

$$\eta = \frac{|S_{21}|^2}{1 - |S_{11}|^2} \times 100\%. \tag{19}$$

By tuning the space s between the loop and disk in the transmitter and receiver, the impedance matching and maximal efficiency conditions were attained for each specific separation d [29].

5.2 NR source and WPT system prototypes fabrication

The dielectric disk of the NR source was fabricated from the bulk ferroelectric composite ceramics based on mixtures of BaTiO$_3$/SrTiO$_3$ powders with Mg-containing additives such as Mg$_2$TiO$_4$, MgO, and the mixture of Mg$_2$TiO$_4$–MgO [32, 33, 37]. The proper ratio of the mixture revealed the ceramic material with colossal permittivity $\varepsilon = 1000$ and low loss factor tan $\delta = 2.5 \times 10^{-4}$. The dielectric disk radius and height are $R = 42 \pm 0.05$ mm and $h = 4.2 \pm 0.05$ mm, respectively. In the fabrication process of the NR source prototype, we replaced the copper loop made of wire by a planar design of the loop (not shown in the figures). It was fabricated using the printed circuit board technology on Rogers RO3003 substrate with the thickness of 0.762 mm and copper metalization of 18 μm. The radius of the loop is $R_0 = 36$ mm, the width of the loop conductor is 4 mm. To connect the loop to a measurement equipment, an SMA connector was mounted to the contact pads created in the 1 mm slit of the loop. To fix the dielectric disk and the loop a special holder was fabricated from ABS plastic by means of 3D printing technique. The holder provides the possibility to tune the distance s needed for the impedance matching at later stages.

The WPT system prototype was implemented using two identical NR sources fabricated as described above (see Figure 5b). To fix the holders of the NR electric sources and organize the WPT system we used a screw-nut fastener made of ABC plastic. This design helps to quickly and accurately change the separation d between the transmitter and receiver of the WPT system.

5.3 Experimental methods

The EM characteristics of the NR source and WPT system were experimentally studied by means of S-parameters and near-field measurements. A Vector Network Analyzer (VNA) ZVB20 was used in the measurements. The investigations were done at 1 dBm output power from the VNA. The NR source reflection coefficient was measured by the direct connection of the prototype the VNA port.

To study the magnetic field distribution above the NR source prototype, the near-field scanning procedure was used [38]. The prototype was connected to the first port of the VNA. A small magnetic probe was used to scan the magnetic field 5 mm above the disk of the prototype. The probe was mounted to an arm of the 3-axis scanner and connected to the second port of the VNA to detect the signal above the disk. The scanner changed the position with a chosen step and measured the transmission coefficient. The magnetic field distributions demonstrated in Figures 2c and 4d were post-processed from the measured data, where the scanner steps were set as 1 and 10 mm, respectively.

To measure the S-parameters of the WPT system the transmitter and receiver of the prototype were connected to the first and second ports of the VNA, respectively. The measured data were used to calculate the WPT efficiency of the system using Eq. (1). The measurements were performed for separations d from 0 to 11 cm with 0.5 cm step. To obtain the maximal WPT efficiency for every separation d, we employed a matching technique. We finely changed the distance s between the dielectric disk and loop reaching that both reflection coefficients $|S_{11}|$ and $|S_{22}|$ are below -20 dB, thus satisfying the impedance matching condition [29]. The obtained PTE is plotted in Figure 7.

References

[1] J. H. Kim, H. S. Lee, G. H. An, et al., "Dielectric nanowire hybrids for plasmon-enhanced light—matter interaction in 2d semiconductors," *ACS Nano*, vol. 14, no. 9, pp. 11985—11994, 2020.

[2] N. S. Mueller, Y. Okamura, B. G. Vieira, et al., "Deep strong light—matter coupling in plasmonic nanoparticle crystals," *Nature*, vol. 583, no. 7818, pp. 780—784, 2020.

[3] P. Forn-Díaz, L. Lamata, E. Rico, J. Kono, and E. Solano, "Ultrastrong coupling regimes of light-matter interaction," *Rev. Mod. Phys.*, vol. 91, no. 2, p. 025005, 2019.

[4] A. F. Kockum, A. Miranowicz, S. De Liberato, S. Savasta, and F. Nori, "Ultrastrong coupling between light and matter," *Nat. Rev. Phys.*, vol. 1, no. 1, pp. 19—40, 2019.

[5] K. Koshelev, G. Favraud, A. Bogdanov, Y. Kivshar, and A. Fratalocchi, "Nonradiating photonics with resonant dielectric nanostructures," *Nanophotonics*, vol. 8, no. 5, pp. 725—745, 2019.

[6] Y.-H. Deng, Z.-J. Yang, M.-L. Hu, X.-J. Du, and J. He, "Boosting an anapole mode response through electromagnetic interactions beyond near-field limit in individual all-dielectric disk-ring nanostructures," *New J. Phys.*, vol. 23, p. 023004, 2021.

[7] K. V. Baryshnikova, D. A. Smirnova, B. S. Luk'yanchuk, and Y. S. Kivshar, "Optical anapoles: concepts and applications," *Adv. Opt. Mater.*, vol. 7, no. 14, p. 1801350, 2019.

[8] A. A. Bogdanov, K. L. Koshelev, P. V. Kapitanova, et al., "Bound states in the continuum and Fano resonances in the strong mode coupling regime," *Adv. Photonics*, vol. 1, no. 1, pp. 1—12, 2019.

[9] K. Koshelev, S. Kruk, E. Melik-Gaykazyan, et al., "Subwavelength dielectric resonators for nonlinear nanophotonics," *Science*, vol. 367, no. 6475, pp. 288—292, 2020.

[10] A. E. Miroshnichenko, A. B. Evlyukhin, Y. F. Yu, et al., "Nonradiating anapole modes in dielectric nanoparticles," *Nat. Commun.*, vol. 6, no. 1, pp. 1—8, 2015.

[11] J. S. T. Gongora, A. E. Miroshnichenko, Y. S. Kivshar, and A. Fratalocchi, "Anapole nanolasers for mode-locking and

ultrafast pulse generation," *Nat. Commun.*, vol. 8, no. 1, pp. 1–9, 2017.

[12] T. C. Huang, B. X. Wang, W. B. Zhang, and C. Y. Zhao, *Ultracompact Energy Transfer in Anapole-Based Metachains*, 2021, arXiv:2103.01457v1 [physics.optics].

[13] C. W. Hsu, B. Zhen, A. D. Stone, J. D. Joannopoulos, and M. Soljačić, "Bound states in the continuum," *Nat. Rev. Mater.*, vol. 1, no. 9, pp. 1–13, 2016.

[14] V. Savinov, N. Papasimakis, D. Tsai, and N. Zheludev, "Optical anapoles," *Commun. Phys.*, vol. 2, no. 1, pp. 1–4, 2019.

[15] J. A. Parker, H. Sugimoto, B. Coe, et al., "Excitation of nonradiating anapoles in dielectric nanospheres," *Phys. Rev. Lett.*, vol. 124, no. 9, p. 097402, 2020.

[16] P. Kapitanova, E. Zanganeh, N. Pavlov, et al., "Seeing the unseen: experimental observation of magnetic anapole state inside a high-index dielectric particle," *Ann. Phys.*, vol. 532, no. 12, p. 2000293, 2020.

[17] V. A. Zenin, A. B. Evlyukhin, S. M. Novikov, et al., "Direct amplitude-phase near-field observation of higher-order anapole states," *Nano Lett.*, vol. 17, no. 11, pp. 7152–7159, 2017.

[18] A. Canós Valero, E. A. Gurvitz, F. A. Benimetskiy, et al., "Theory, observation, and ultrafast response of the hybrid anapole regime in light scattering," *Laser Photon Rev.*, vol. 15, p. 2100114, 2021.

[19] A. Shevchenko, V. Vashistha, M. Nyman, and M. Kaivola, "Electromagnetic anapoles of a cartesian expansion of localized electric currents," *Phys. Rev. Res.*, vol. 2, no. 4, p. 042043, 2020.

[20] N. A. Nemkov, I. V. Stenishchev, and A. A. Basharin, "Nontrivial nonradiating all-dielectric anapole," *Sci. Rep.*, vol. 7, no. 1, pp. 1–9, 2017.

[21] J. R. Zurita-Sánchez, "Anapole arising from a mie scatterer with dipole excitation," *Phys. Rev. Res.*, vol. 1, no. 3, p. 033064, 2019.

[22] E. Zanganeh, A. Evlyukhin, A. Miroshnichenko, M. Song, E. Nenasheva, and P. Kapitanova, "Anapole meta-atoms: nonradiating electric and magnetic sources," *Phys. Rev. Lett.*, vol. 127, no. 9, p. 096804, 2021.

[23] O. Keller, "Attached and radiated electromagnetic fields of an electric point dipole," *J. Opt. Soc. Am. B*, vol. 16, no. 5, pp. 835–847, 1999.

[24] M. Song, P. Belov, and P. Kapitanova, "Wireless power transfer inspired by the modern trends in electromagnetics," *Appl. Phys. Rev.*, vol. 4, p. 021102, 2017.

[25] M. Song, P. Jayathurathnage, E. Zanganeh, et al., "Wireless power transfer based on novel physical concepts," *Nat. Electron.*, vol. 4, pp. 707–716, 2021.

[26] A. Kurs, A. Karalis, R. Moffatt, J. D. Joannopoulos, P. Fisher, and M. Soljačić, "Wireless power transfer via strongly coupled magnetic resonances," *Science*, vol. 317, no. 5834, pp. 83–86, 2007.

[27] E. Shamonina, L. Solymar, and V. Kalinin, "On wireless power transfer between coils in the presence of radiation," *J. Phys. D: Appl. Phys.*, vol. 54, p. 405502, 2021.

[28] M. Song, I. Iorsh, P. Kapitanova, E. Nenasheva, and P. Belov, "Wireless power transfer based on magnetic quadrupole coupling in dielectric resonators," *Appl. Phys. Lett.*, vol. 108, no. 2, p. 023902, 2016.

[29] M. Song, P. Belov, and P. Kapitanova, "Wireless power transfer based on dielectric resonators with colossal permittivity," *Appl. Phys. Lett.*, vol. 109, no. 22, p. 223902, 2016.

[30] Y. Xie, Z. Zhang, Y. Lin, T. Feng, and Y. Xu, "Magnetic quasi-bound state in the continuum for wireless power transfer," *Phys. Rev. Appl.*, vol. 15, p. 044024, 2021.

[31] V. R. Tuz, V. Dmitriev, and A. B. Evlyukhin, "Antitoroidic and toroidic orders in all-dielectric metasurfaces for optical near-field manipulation," *ACS Appl. Nano Mater.*, vol. 3, no. 11, pp. 11315–11325, 2020.

[32] E. Nenasheva, N. Kartenko, I. Gaidamaka, et al., "Low loss microwave ferroelectric ceramics for high power tunable devices," *J. Eur. Ceram. Soc.*, vol. 30, no. 2, pp. 395–400, 2010.

[33] E. Nenasheva, N. Kartenko, I. Gaidamaka, S. Redozubov, A. Kozyrev, and A. Kanareykin, "Low permittivity ferroelectric composite ceramics for tunable applications," *Ferroelectrics*, vol. 506, no. 1, pp. 174–183, 2017.

[34] A. B. Evlyukhin, T. Fischer, C. Reinhardt, and B. N. Chichkov, "Optical theorem and multipole scattering of light by arbitrarily shaped nanoparticles," *Phys. Rev. B*, vol. 94, no. 20, p. 205434, 2016.

[35] E. A. Gurvitz, K. S. Ladutenko, P. A. Dergachev, A. B. Evlyukhin, A. E. Miroshnichenko, and A. S. Shalin, "The high-order toroidal moments and anapole states in all-dielectric photonics," *Laser Photon. Rev.*, vol. 13, no. 5, p. 1800266, 2019.

[36] R. Alaee, C. Rockstuhl, and I. Fernandez-Corbaton, "An electromagnetic multipole expansion beyond the long-wavelength approximation," *Opt. Commun.*, vol. 407, pp. 17–21, 2018.

[37] N. Shipman, J. Bastard, E. Nenasheva, et al., "Jacow: a ferroelectric fast reactive tuner for superconducting cavities," Tech. Rep., 2019.

[38] N. Pavlov, I. Stenishchev, A. Ospanova, P. Belov, P. Kapitanova, and A. Basharin, "Toroidal dipole mode observation in situ," *Phys. Status Solidi B*, vol. 257, no. 3, p. 1900406, 2020.